Simulations of Nanoscale Room-Temperature Waveguide-Coupled Single-Photon Avalanche Detectors for Silicon-Photonic Sensing and Quantum Applications

R. A. Soref[1], *F. De Leonardis*[2] *and V. M. N. Passaro*[2,*]

[1]Department of Engineering, The University of Massachusetts, Boston, Massachusetts, 02125 United States

[2]Photonics Research Group, Dipartimento di Ingegneria Elettrica e dell'Informazione, Politecnico di Bari, Via Edoardo Orabona n. 4, 70125 Bari, Italy [*]vittorio.passaro@poliba.it

FABRICATION PROCESSES FOR SPADS

There are reasons to believe that the SPAD fabrication is quite compatible with present-day silicon photonics fabrication. There is already an industry-standard epitaxial-Germanium-on-SOI photodetector (PD) being manufactured routinely in the "CMOS photonics" foundry (a PD that is multi-photon or conventional). Regarding the related GeSn epitaxy needed here, the GeSn chemical-vapor deposition has two chemical precursors rather than the single precursor employed

for elemental Ge CVD. Successful experiments on buffer-less growth of GeSn on Si made use of the germane and stannane precursors [1]. So, the GeSn CVD is arguably not very different from the Ge germane CVD, and that is why there is a pathway for GeSn photodetectors (conventional at first, and single-photon later) to enter the foundry environment. Also, recent developments within electronics foundries have shown that GeSn is successfully incorporated as a transistor source and drain. For all the foregoing reasons, the on-going world-wide developments being made in the GeSn art provide a "practical trajectory for GeSn foundry entry" during the next few years.

Going into more specifics about the SPAD fabrication, there is a close analogy between the present device and the various experimental Ge-on-Si SPADs discussed in the recent literature. Specifically, a paper by Ke *et al.* [2], compares fabrication of the Ge-on-Si Geiger-SPADs by direct epitaxial growth, by two-step epi growth and by direct wafer bonding. All three methods were viable, but the wafer- bonded SPADs exhibited extremely low DCR and dark current. In our opinion, the same three options for fabricating our GeSn/Si SPADs (the PIPIN stack of Fig. 1 of the main paper) are available to process engineers: one-step epi, two-step epi and GeSn wafer bonding. An example of the two-step epi is to grow a 50-nm "seed layer" of i-Ge upon the P+ Si before growing the i-GeSn, providing a strategy to reduce threading dislocations in the i-GeSn.

For the wafer bonding, the donating wafer could be SOI upon which a high-quality Ge buffer has been grown on the silicon before the low-defect-density crystalline i-GeSn film is then grown on that Ge. Bonding to the second SOI "device wafer" is then performed. The device wafer contains (at multiple sites generally) the partially constructed SPAD devices -the selective-area epi silicon PIN structures, as well as the Si strip waveguides. To provide a planar wafer-to-wafer

bond surface, strip recesses are etched in the donating GeSn; features that match exactly the protruding Si strips in the device wafer. The authors of [2] point out the risk of generating an unwanted 0.5 nm GeO_2 layer at the bond interface, but they show that an ultrathin few-nm film of Si (grown on the i-GeSn donor wafer in our case) could prevent that thin tunnel oxide. In summary, several fabrication procedures appear practical for our proposed devices, with the bonding technique being overall more difficult, but yet more rewarding for its very reduced concentration of threading dislocations (TDs) and bulk traps, the low density needed for low DCR. To quantify this, we estimate that wafer bonding offers an order-of-magnitude lower TD density than direct epi.

Regarding the band-offsets and band alignment at the GeSn/P-Si surface, if we look at the Δ-valleys in the conduction band (which always lie lower in energy than the CB L-valleys), then this band alignment is usually Type II, with a larger valence-band HH to HH offset than the fairly small Δ-to-Δ conduction-band offset. Considering the L-valleys, the band alignment is typically Type I.

GeSn ABSORPTION

In order to obtain most of the parameters for the $Ge_{1-x}Sn_x$ material system, linear interpolations among Ge and α-Sn parameters have been used, with the exception of the bandgaps [3]. The physical parameters used for our investigations are listed in Table I. However, as outlined in [3]-[5], a better estimation for the energy-band gaps at the conduction Γ, L, and X points of the

unstrained $Ge_{1-x}Sn_x$ alloy can be achieved as in Eq. (S1) by using the quadratic polynomials including the significant bowing effects ($b_{GeSn}^{(n)}$):

$$E^{(n)}\left(Ge_{1-x}Sn_x\right)=(1-x)E^{(n)}\left(Ge\right)+xE^{(n)}\left(GeSn\right)-b_{GeSn}^{(n)}x(1-x) \quad \text{(S1)}$$

In Eq. (S1), n= Γ, L, X and the bowing parameter values are $b_{GeSn}^{(\Gamma)}$ =1.94 (2.92) [3], ([4]) and $b_{GeSn}^{(L)}$=1.23 [3].

Table S1. Physical Parameters of Ge and α-Sn.

Materials	**Parameters (from ref. [3])**								
	m_c/m_0 (Γ)	m_t/m_0 (L)	m_l/m_0 (L)	m_{v1}/m_0	m_{v2}/m_0	$E(\Gamma)$ [eV]	$E(L)$ [eV]	$E(X)$ [eV]	ε_r
Ge	0.038	0.0807	1.57	0.28	0.044	0.805	0.7013	0.9013	16.2
α-Sn	0.058	0.075	1.478	0.3	0.038	-0.4102	0.14	0.9102	24

A detailed analysis of absorption coefficient and refractive index for $Ge_{1-x}Sn_x$ alloys is presented in [4], where semi-analytical formulae have been developed by fitting the spectroscopic ellipsometry data. Since we are interested in maximizing the absorption coefficient, we focus our attention to the direct transition. Thus, according to ref. [4], the absorption coefficient near the bandgap can be written as:

$$\alpha(\hbar\omega) = \frac{A\sqrt{\hbar\omega - E^{(\Gamma)}\left(Ge_{1-x}Sn_x\right)}}{\hbar\omega} \quad \text{for} \quad \hbar\omega \geq E^{(\Gamma)}\left(Ge_{1-x}Sn_x\right) + 0.5\Delta E \qquad \text{(S2)}$$

where ΔE=10.58 meV is the Urbach width and A= 3.68×10^4 [cm^{-1} eV$^{1/2}$] is a fitting constant.

In Fig. S1 we show the absorption coefficient as a function of the Sn concentration for two different photon energies, 0.80 eV (λ=1550 nm) and 0.62 eV (λ=2000 nm).

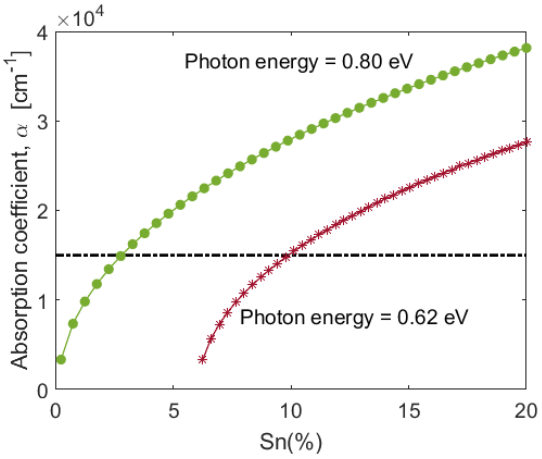

Figure S1. Direct absorption coefficient as a function of Sn title for photon energy of 0.8 eV and 0.62 eV, respectively.

The curves indicate that an absorption coefficient as large as α=15000 cm^{-1} can be obtained by setting x~3% and ~10% for λ= 1550 nm and 2000 nm, respectively.

REFERENCES

1. C. S. Cook, S. Zollner, M. R. Bauer, P. Aella, J. Kouvetakis, J. Menendez, "Optical constants and interband transitions of $Ge_{1-x}Sn_x$ alloys (x< 0.2) grown on Si by UHV-CVD," *Thin Solid Films*, **455**, 217-221, 2004.

2. S. Ke, S. Lin, D. Mao, Y. Ye, X. Ji, W. Huang, C. Li, S. Chen, "Design of wafer-bonded structures for near room temperature Geiger-mode operation of germanium on silicon single-photon avalanche photodiode," *Appl. Optics*, **56**(16), 4646-4653, 2017.

3. G. E. Chang, S. W. Chang, S. L. Chuang, "Strain-balanced Ge_zSn_{1-z}-$Si_xGe_ySn_{1-x-y}$ multiple-quantum well lasers," *IEEE J. Quantum Electron.* **46**, 1813-1820, 2010.

4. H. Tran, W. Du, S. A. Ghetmiri, A. Mosleh, G. Sun, R. A. Soref, J. Margetis, J. Tolle, B. Li, H. A. Naseem, S.Q. Yu, "Systematic study of Ge1-xSnx absorption coefficient and refractive index for the device applications of Si-based optoelectronics," *J. Appl. Phys.* **119**, 103106, 2016.

5. P. Moontragoon, R. A. Soref, Z. Ikonic, "The direct and indirect bandgaps of unstrained $Si_xGe_{1-x-y}Sn_y$ and their photonic device applications," *J. Appl. Phys.* **112**, 073106, 2012.